Available online at www.sciencedirect.com

ScienceDirect

materialstoday: PROCEEDINGS
www.materialstoday.com/proceedings

Materials Today: Proceedings 1 (2014) 11 – 16

The 1st International Joint Mini-Symposium on Advanced Coatings between Indiana University-Purdue University Indianapolis and Changwon National University

Microstructural non-uniformity and mechanical property of air plasma-sprayed dense lanthanum zirconate thermal barrier coating

Jing Zhang[a]*, Xingye Guo[a], Yeon-Gil Jung[b], Li Li[c], James Knapp[c]

[a]*Department of Mechanical Engineering, Indiana University-Purdue University Indianapolis, Indianapolis, IN46202, USA*
[b]*Department of Materials Science & Engineering, Changwon National University, Changwon, Gyeongnam 641-773, Korea*
[c]*Praxair Surface Technologies Inc., Indianapolis, IN46222, USA*

Abstract

Lanthanum zirconate is a promising thermal barrier coating material. In this work, imaging technique was used to characterize the microstructural non-uniformity of the coating. The imaging analyses revealed that, along the thickness of the coating, the cracks were primarily horizontal in the top and middle regions, while vertical cracks became dominant in the bottom region. The calculated porosities showed a non-uniformity (4.8%, 5.3%, and 5.5% in the top, middle, and bottom regions, respectively). They were lower than the experimentally measured one, 7.53%, using the Archimedes method. This is because imaging analysis does not take internal porosity into account. Additionally, the measured Vickers hardness was 5.51±0.25 GPa, nanoindentation hardness was 8.8±2.1 GPa, and Young's modulus was 156.00±10.03 GPa.

Selection and Peer-review under responsibility of the Chairs of The 1st International Joint Mini-Symposium on Advanced Coatings between Indiana University-Purdue University Indianapolis and Changwon National University, Indianapolis.

Keywords: Lanthanum zirconate; mechanical property; Fast Fourier Transform; microstructure; air plasma spray

* Corresponding author. Tel.:+1-317-278-7186; fax: +1-317-274-9744.
E-mail address: jz29@iupui.edu

Selection and Peer-review under responsibility of the Chairs of The 1st International Joint Mini-Symposium on Advanced Coatings between Indiana University-Purdue University Indianapolis and Changwon National University, Indianapolis.
doi:10.1016/j.matpr.2014.09.003

1. Introduction

Lanthanum zirconate ($La_2Zr_2O_7$, LZ) is a promising material as thermal barrier coating (TBC) on industrial gas turbines or in aerospace applications. Compared with current the state-of-the-art TBC material 8YSZ (8 mol% Y_2O_3 fully stabilized ZrO_2), $La_2Zr_2O_7$ has several attributes that make it more attractive for high temperature applications: (1) lanthanum zirconate is a stable, ordered pyrochlore to the melting temperature of 2295±10 ^oC, as shown in the La_2O_3-ZrO_2 phase diagram [1] (Figure 1). The stability region ranges from approximately 33 to 35 mol. % La_2O_3 at 1500 ^oC [2]. This is because lanthanum zirconate can accommodate a large amount of vacancies at the La^{3+}, Zr^{4+}, and O^{2-} sites [3]; (2) lanthanum zirconate has a low bulk thermal conductivity of 1.56 W/m-K [3]; and (3) it has a better sintering resistance than 8YSZ at elevated temperatures.

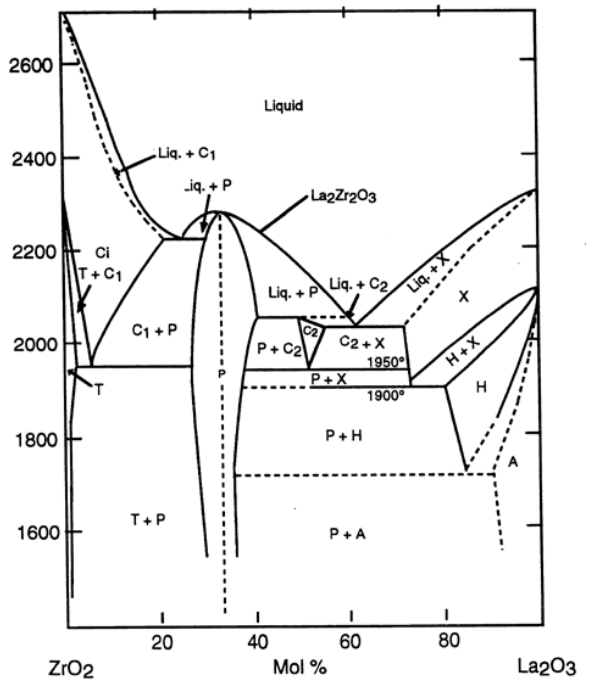

Figure 1: Phase diagram of La_2O_3 – ZrO_2 [1].

A few recent publications [4, 5] have provided good review of the application of lanthanum zirconate for thermal barrier coating applications. In this work, imaging technique will be used to characterize the microstructural non-uniformity of the coating. The orientation of the cracks and porosity distribution will be analyzed using the Fast Fourier Transform (FFT) technique. The hardness and Young's modulus will also be experimentally measured.

2. Experimental

2.1. Materials and spray conditions

Lanthanum zirconate powders (Praxair Surface Technologies, Indianapolis, IN) with a medium diameter, D_{50}, of 65 μm were atmospheric plasma sprayed (APS'ed) onto Haynes 188 substrate using a Praxair Surface Technologies

patented plasma torch. The APS processing parameters (e.g., torch current, standoff distance, powder feed rate etc) were described previously [6]. In essence, the processing parameters were adjusted to produce desirable porosity in the coatings. In this work, a representative dense coating was presented showing its the microstructure un-uniformity and mechanical properties.

2.2. Microstructure

The coating samples were removed from the substrate after spray to examine the microstructure. The free standing samples were processed to observe the cross-sectional microstructure and to evaluate mechanical properties. The microstructures of the samples were characterized with a scanning electron microscope (SEM; Model JSM–5610, JEOL, Japan).

2.3 Porosity and hardness

The bulk density of the sintered specimens was measured by the Archimedes method [7], and the relative density and porosity were calculated using a theoretical full density value (6.0 g/cm^3).

To examine the localized relative density in the top, middle and bottom regions of the coating, image processing technique [8] was used using the SEM images to derive the porosity at the top, middle, and bottom regions of the coating.

The hardness values of the top coats were determined using a micro indenter (HM-114, Mitutoyo Corp., Japan) with a Vickers tip for a load of 3 N. To obtain more reliable values, 15 points were tested for each result. Additionally, nanoindentation was carried out on the sectional planes of each TBC to determine elastic modulus using a nanoindenter (Nanoinstruments, MTS Systems Corp., Eden Prairie, USA) employing a Berkovich tip (radius < 100 nm).

The two-dimensional fast Fourier Transform (FFT) was used to quantitatively analyze the SEM images for localized porosity and crack anisotropy. The SEM gray image data for fast Fourier Transform were pretreated to derive the binary (black and white) images in the region of interest (ROI). In FFT, the gray level of each pixel of the image is represented by a function, $g(x,y)$, where x and y are the Cartesian coordinates of a pixel point. The 2D discrete Fourier transform $g(x,y)$ is $F(n,m)$ and expressed as [9]

$$F(n,m) = \frac{1}{N^2}\sum_{x=0}^{N-1}\sum_{y=0}^{N-1} g(x,y)\exp\{-\frac{2\pi i(xn+ym)}{N}\} \quad (1)$$

where n and m are spatial frequencies corresponding to the x-axis and the y-axis of the ROI binary images. The value N is the size of a two-dimensional square array and should be a power of 2 for the FFT algorithm. The preferred orientation in the image is represented by a bright peak in the power spectrum $|F(n,m)|^2$ around the origin of the frequency transform.

3. Results and discussion

The backscattered SEM image of cross-sectional view of the TBC specimen is shown in Figure 2, which shows a 500 micron-thick dense microstructure with a few vertical cracks.

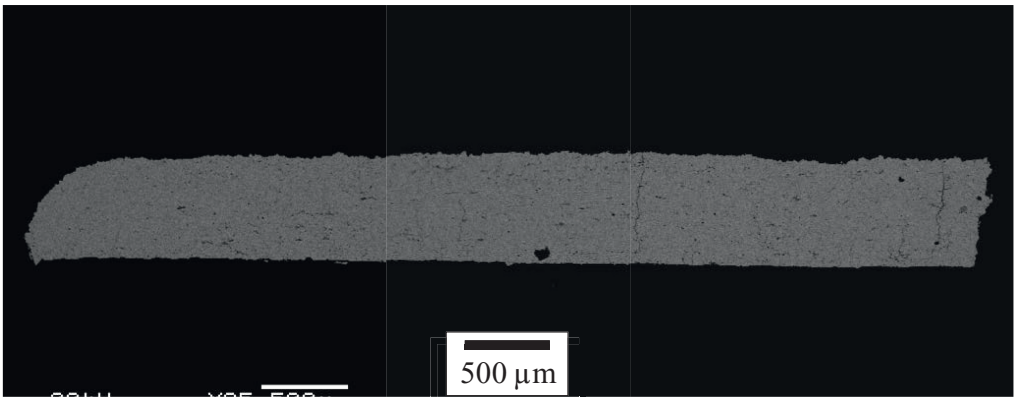

Figure 2: Backscattered SEM image of cross-sectional view of the TBC free standing sample.

The higher magnification SEM images of the coating at the top, middle, and bottom regions are given in Table 1. The top region of the coating shows a typical APS'd sample microstructure. Horizontal cracks and grains were produced. The middle and bottom regions, however, exhibit mixture vertical and horizontal cracks. The bottom one, which is close to the bond coats was dominated by vertical cracks.

Table 1: SEM image, ROI binary image, FFT, and computed porosity of the TBC sample in Figure 2.

	SEM image	ROI binary image	FFT	Porosity
top	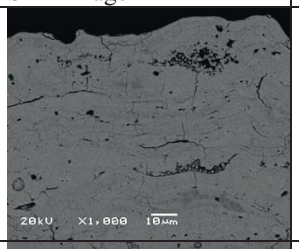	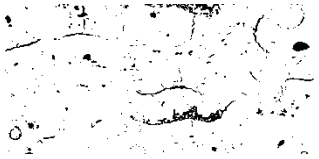		4.8%
middle	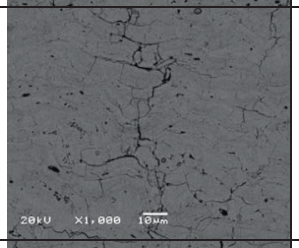	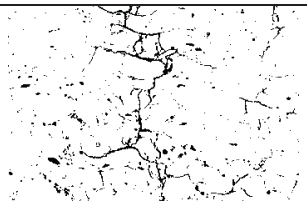	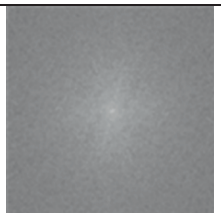	5.3%
bottom	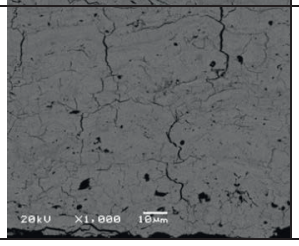	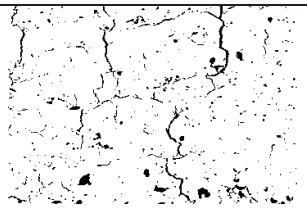	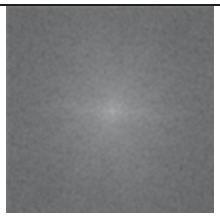	5.5%

The un-uniformity and anisotropy features of the coatings are revealed in the image processed data in Table 1. The porosities of the coating were calculated using the ROI binary images. In a ROI binary image, black pixels are counted as pores and the white pixels are solid phases. The porosities at the top, middle, and bottom regions of the coating were calculated as 4.8%, 5.3%, and 5.5%, respectively. Therefore, there is a porosity gradient through the thickness of the coating.

The porosity was also experimentally determined using the Archimedes method, and the measured porosity was 7.53%. The experimentally measured porosity was higher than that calculated from the 2D images in Table 1. This is because the 2D image based measurements only count surface porosity, but not internal porosity, thus underestimated the results. With reconstructed 3D images, a more accurate porosity will be expected. Another note is that the Archimedes method only gives overall porosity of a given sample. Image based porosity provides localized information about porosity distribution.

Fast Fourier Transform of the ROI binary images is given in Table 1. For the top and middle regions, the bright peaks in FFT were slightly tilted about 5^{o} to the right of the vertical direction, suggesting most cracks oriented in the horizontal direction. In contrast, the bottom FFT shows a horizontal bright peak, indicating cracks were primarily vertical. Therefore, FFT provides an effective way to characterize the non-uniformity features of the TBC microstructures.

Both Vickers microindentation and nanoindentation tests were conducted to characterize the hardness of the coating. The measured Vickers hardness was 5.51±0.25 GPa, and nanoindentation hardness was 8.8±2.1 GPa. The nanoindentation hardness is higher than the Vickers hardness, due to localized indentation characteristics in nanoindentation. The Young's modulus of the coating, derived from nanoindentation test, is shown in Figure 3. The Young's modulus decreased with increasing indentation depth, as expected in a typical indentation test. The average of the Young's modulus was 156.00±10.03 GPa.

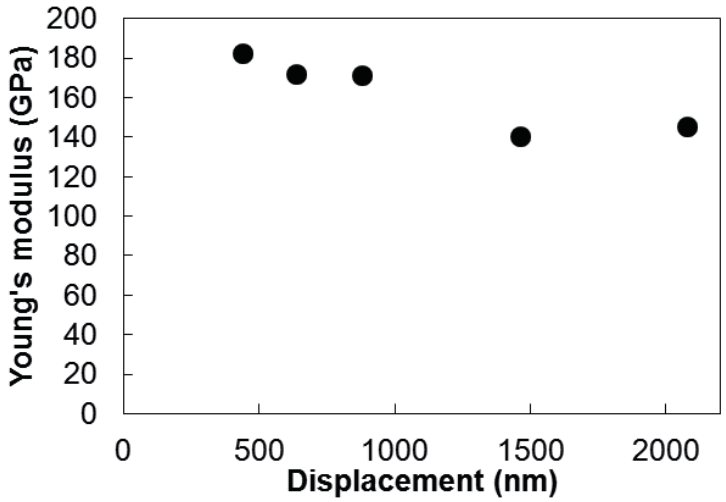

Figure 3: Young's modulus as a function of nanoindentation displacement.

4. Conclusion

Imaging technique has been used to characterize the microstructural non-uniformity of the lanthanum zirconate thermal barrier coating. The imaging analyses revealed that, along the thickness of the coating, the cracks were primarily horizontal in the top and middle regions, while vertical cracks became dominant in the bottom region. The

calculated porosities showed a non-uniformity (4.8%, 5.3%, and 5.5% in the top, middle, and bottom regions, respectively). They were lower than the experimentally measured one, 7.53%. This is because imaging analysis does not take internal porosity into account. Additionally, the measured Vickers hardness was 5.51±0.25 GPa, and nanoindentation hardness was 8.8±2.1 GPa. The Young's modulus was 156.00±10.03 GPa.

Acknowledgement

The authors would like to acknowledge the financial support provided by DOE (Grant No. DE-FE0008868, program manager Richard Dunst). Y.G.J. acknowledges the support provided by the National Research Foundation of Korea (NRF) grant funded by the Korean Government (MSIP) (No. 2011-0030058) and the Human Resources Development Program (No. 20134030200220) of the Korea Institute of Energy Technology Evaluation and Planning (KETEP) grant funded by the Korean Government Ministry of Trade, Industry and Energy.

References

1. Maloney, M.J., *A ceramic surface coatings has a cubic pyrochlore structure*, 2000, US Patent US6117560 A.
2. Radha, A.V., S.V. Ushakov, and A. Navrotsky, *Thermochemistry of lanthanum zirconate pyrochlore.* Journal of Materials Research, 2009. **24**(11): p. 3350-3357.
3. Mauer, G., et al., *Plasma-Sprayed Thermal Barrier Coatings: New Materials, Processing Issues, and Solutions.* Journal of Thermal Spray Technology, 2013. **22**(5): p. 646-658.
4. Cao, X.Q., R. Vassen, and D. Stoever, *Ceramic materials for thermal barrier coatings.* Journal of the European Ceramic Society, 2004. **24**(1): p. 1-10.
5. Bansal, N.P. and D. Zhu, *Effects of doping on thermal conductivity of pyrochlore oxides for advanced thermal barrier coatings.* Materials Science and Engineering: A, 2007. **459**(1): p. 192-195.
6. Zhang, J. *Novel Functional Graded Thermal Barrier Coatings in Coal-fired Power Plant Turbines*. 2003 Available from: http://www.netl.doe.gov/File%20Library/events/2013/hbcu-ucr/Novel-Functional_Zhang--Compatibility-Mode-.pdf.
7. Zhang, Y., Y. Liu, and M. Liu, *Nanostructured Columnar Tin Oxide Thin Film Electrode for Lithium Ion Batteries.* Chemistry of Materials, 2006. **18**(19): p. 4643-4646.
8. Schneider, C.A., W.S. Rasband, and K.W. Eliceiri, *NIH Image to ImageJ: 25 years of image analysis.* Nat Meth, 2012. **9**(7): p. 671-675.
9. Bankman, I., *Handbook of Medical Image Processing and Analysis*2008: Academic Press.